PCCP

PAPER

View Article Online
View Journal | View Issue

Check for updates

Cite this: *Phys. Chem. Chem. Phys.*, 2024, **26**, 11459

Reverse intersystem crossing mechanisms in doped triangulenes†

Asier E. Izu, [ab] Jon M. Matxain [ab] and David Casanova *[ac]

Received 23rd January 2024,
Accepted 23rd March 2024

DOI: 10.1039/d4cp00304g

rsc.li/pccp

Thermally activated delayed fluorescence (TADF) has emerged as one of the most promising strategies in the quest for organic light emitting diodes with optimal performance. This computational study dissects the mechanistic intricacies of the central photophysical step, reverse intersystem crossing (rISC) in N and B doped triangulenes as potential multi-resonance TADF compounds. Optimal molecular patterns conducive to efficient rISC, encompassing dopant atom size, number, and distribution, are identified. Additionally, we assess various electronic structure methods for characterizing TADF-relevant molecular systems. The findings identify the distinct role of the direct and mediated mechanisms in rISC, and provide insights into the design of advanced TADF chromophores for next-generation OLED technology.

Open Access Article. Published on 25 März 2024. Downloaded on 06.02.26 16:58:20.
This article is licensed under a Creative Commons Attribution 3.0 Unported Licence.

1 Introduction

Organic light emitting diodes (OLEDs) have revolutionized the technological market, finding ubiquitous application as luminescent displays in devices such as televisions and smartphones.[1–3] The pursuit of better performing OLED devices has therefore garnered significant attention.

In OLEDs, the recombination of charges leads to the formation of singlet and triplet states in a 1 : 3 ratio, imposing a stringent limitation on internal quantum efficiency. To mitigate non-radiative losses from the population of the (dark) triplet state manifold, two primary strategies have been proposed, each with the potential to achieve 100% internal quantum efficiency: doping with phosphorescent emitters[4–6] and thermally activated delayed fluorescence (TADF).[7–10] The former employs organometallic complexes to attain the necessary high spin–orbit coupling (SOC), allowing triplet states to undergo (phosphorescent) radiative decay. In contrast, TADF relies on organic molecules that recycle their non-radiative triplet excited states to fluorescence emissive singlets *via* reverse intersystem crossing (rISC) and thermal ambient energy, eliminating the need for expensive and toxic transition metals, *e.g.*, Ir or Pt, used in phosphorescent OLEDs.

The TADF phenomenon can be broken down into two main steps: triplet-to-singlet rISC and fluorescence from the lowest excited singlet state (S_1). Efficient population of S_1 through rISC necessitates a small energy difference between the excited singlet and triplet states ($\Delta E_{ST} = E(S_1) - E(T_1)$), *i.e.*, in the order of the thermal energy, and a strong coupling between the initial (spin triplet) and final (spin singlet) states, with SOC being the most common relativistic interaction connecting the two spin manifolds in organic compounds.[11] Additionally, a good TADF chromophore must exhibit strong luminescence from S_1, which can be quantified by the area of the emission band (oscillator strength).

The most commonly utilized strategy for designing systems with narrow T_1/S_1 energy gaps relies on the correlation between ΔE_{ST} and the exchange interaction among the frontier molecular orbitals (MOs). Vanishing orbital exchange can be achieved in molecules featuring weakly coupled and spatially separated donor and acceptor units. This situation typically involves T_1 and S_1 states holding strong charge transfer (CT) character.[12–16] However, this strategy suffers from a number of drawbacks, primarily small photoluminescence quantum yields (PLQY) and poor color purity. The extensive structural reorganization of CT-character molecular architecture leads to broad emission spectra. Furthermore, CT-character excitations often exhibit small oscillator strengths, resulting in weak radiative emission.[17]

A notable departure from the usual donor–acceptor architecture was proposed by Hatakeyama *et al.*, who designed TADF emitters with triangulene cores incorporating *ortho*-substituted B and N atoms, forming DABNA molecules.[17] These molecules, often referred to as multi-resonance TADF (MR-TADF) compounds, feature a chemical structure that promotes

[a] *Donostia International Physics Center (DIPC), 20018 Donostia, Euskadi, Spain. E-mail: david.casanova@dipc.org*
[b] *Polimero eta Material Aurreratuak: Fisika, Kimika eta Teknologia Saila, Kimika Fakultatea, Euskal Herriko Unibertsitatea (UPV/EHU), PK 1072, 20080 Donostia, Euskadi, Spain*
[c] *IKERBASQUE, Basque Foundation for Science, 48009 Bilbao, Euskadi, Spain*

† Electronic supplementary information (ESI) available: Symmetry point group for the ground state of studied molecules. Singlet and triplet energies computed with different methods. See DOI: https://doi.org/10.1039/d4cp00304g

Open Access Article. Published on 25 März 2024. Downloaded on 06.02.26 16:58:20.
This article is licensed under a Creative Commons Attribution 3.0 Unported Licence.

the localization of the highest occupied and lowest unoccupied MOs (HOMO and LUMO) in different atomic sites. This leads to disjoint HOMO and LUMO, triggering small exchange interactions (small ΔE_{ST}), while still allowing for sizeable $S_0 \leftarrow S_1$ transition dipole moments. Furthermore, the backbone rigidity induces narrow emission bands. These properties have been associated with singlet and triplet states exhibiting a ''short-range/local'' CT character and long-range π-conjugation,[17,18] motivating the ongoing search for new and improved MR-TADF chromophores.[19–23]

The main objective of this study is to elucidate the mechanistic intricacies of rISC in N and B doped triangulenes, which are potential candidates as MR-TADF compounds, through the application of quantum chemistry calculations. Furthermore, we endeavor to pinpoint optimal molecular patterns conducive to efficient rISC, including considerations of size, number, and distribution of dopant atoms. Additionally, our investigation assesses the suitability of various electronic structure methods for computationally characterizing molecular systems relevant to TADF.

The paper is organized as follows. In the first section, we delve into the theoretical expressions employed to characterize the rates of rISC mechanisms and provide an overview of the electronic structure methods investigated for the study of doped triangulenes. The subsequent section presents the results of our exploration into the capabilities of both density functional (DFT) and wave function approaches for the study of 16 triangulene derivatives. We carefully select the optimal methodology and conduct the computational analysis. Finally, in the Conclusions section, we thoroughly discuss the main findings of our investigations.

2 Theory and methodology

2.1 Reverse intersystem crossing rates

The rate of rISC from a triplet state to an excited singlet can be expressed using Fermi's golden rule:

$$k_{\mathrm{rISC}} = \frac{2\pi}{\hbar}|V_{\mathrm{rISC}}|^2 \delta(\Delta E_{\mathrm{ST}}) \tag{1}$$

where V_{rISC} is the coupling between initial (triplet) and final (singlet) states, and $\delta(\Delta E_{\mathrm{ST}})$ is the Franck–Condon weighted density of states within the singlet–triplet energy gap ΔE_{ST}. Eqn (1) indicates that the efficiency of rISC strongly depends on the energy alignment and coupling between the triplet and singlet states. We assume that singlet–triplet couplings in organic compounds, particularly for MR-TADF molecules, are dominated by SOC. Hyperfine interactions (HFI), which may become important between singlet and triplet states with strong CT character,[24,25] are much weaker and can be disregarded. Additionally, it has been shown that rISC can be enhanced by the vibronic coupling of T_1 with higher triplets, known as the spin–vibronic mechanism.[16,26,27] To incorporate this mechanism in our computational methodology, we expand the (first order) coupling between initial and final states (eqn (2)) to second-order perturbation theory[28] (eqn (3)),

$$V_{\mathrm{rISC}}^{(d)} = \langle S_1|\hat{H}_{\mathrm{SO}}|T_1\rangle \tag{2}$$

$$V_{\mathrm{rISC}}^{(m)} = \sum_{n\neq 1} \frac{\langle S_1|\hat{H}_{\mathrm{SO}}|T_n\rangle\langle T_n|\hat{H}_{\mathrm{vib}}|T_1\rangle}{E(T_1) - E(T_n)} \tag{3}$$

where $\hat{H}_{\mathrm{SO}}$ is the spin–orbit Hamiltonian, and the first and second order terms have been labelled according to the two different rISC mechanisms, direct ($V_{\mathrm{rISC}}^{(d)}$) and mediated ($V_{\mathrm{rISC}}^{(m)}$) couplings, respectively. The quantitative assessment of eqn (3) requires the calculation of nonadiabatic couplings between triplet states. Analytic implementations of these couplings are currently available for a variety of electronic structure methods.[29–35] Alternatively, vibronic couplings can be numerically evaluated, for instance through the linear vibronic coupling model.[16] These calculations can be conducted by considering one or a limited set of selected modes as the ones promoting interstate couplings, or with more general formalisms, *e.g.*, with the use of thermal vibration correlation functions.[36] The spin–vibronic (mediated) mechanism is particularly efficient in the presence of higher triplet states with strong SOC with S_1 and not too large energy gaps to T_1. However, the perturbation approach diverges for vanishing T_n/T_1 energy gaps, *i.e.*, on the order of the vibronic coupling or smaller, and should not be applied when $E(T_1) - E(T_n) \to 0$. To overcome this limitation, we assume thermal equilibrium between the N_{T} degenerate or nearly-degenerate lowest triplet states, evaluating the total rISC rate as a weighted sum of individual rates given by the Boltzmann distribution:

$$k_{\mathrm{rISC}} = \sum_{i}^{N_{\mathrm{T}}} p_i k_{\mathrm{rISC}}^{(i)} \tag{4}$$

$$p_i = \frac{e^{-E_i/k_{\mathrm{B}}T}}{\sum_{j}^{N_{\mathrm{T}}} e^{-E_j/k_{\mathrm{B}}T}} \tag{5}$$

where T is the temperature, k_{B} is the Boltzmann constant, and E_i is the energy of the i-th (nearly) degenerate triplet.

Finally, to evaluate rISC in eqn (1), we approximate the Franck–Condon weighted density of states using the Marcus approximation for the high temperature limit:[37]

$$\delta(\Delta E) = \frac{e^{-\frac{(\Delta E+\lambda)^2}{4\lambda k_{\mathrm{B}}T}}}{\sqrt{4\pi\lambda k_{\mathrm{B}}T}} \tag{6}$$

where λ is the reorganization energy.

2.2 Molecular systems and nomenclature

In this study, we examine a series of 16 triangulene nanographene molecules doped with nitrogen and/or boron atoms (Fig. 1). The selection of these compounds is deliberate, aimed at comprehending the influence of molecular size (phenalene or triangulene scaffold), doping quantity, type of doping atoms (B or N), and the distribution of dopants on their potential as MR-TADF molecules.

 This journal is © the Owner Societies 2024

Open Access Article. Published on 25 März 2024. Downloaded on 06.02.26 16:58:20.
This article is licensed under a Creative Commons Attribution 3.0 Unported Licence.

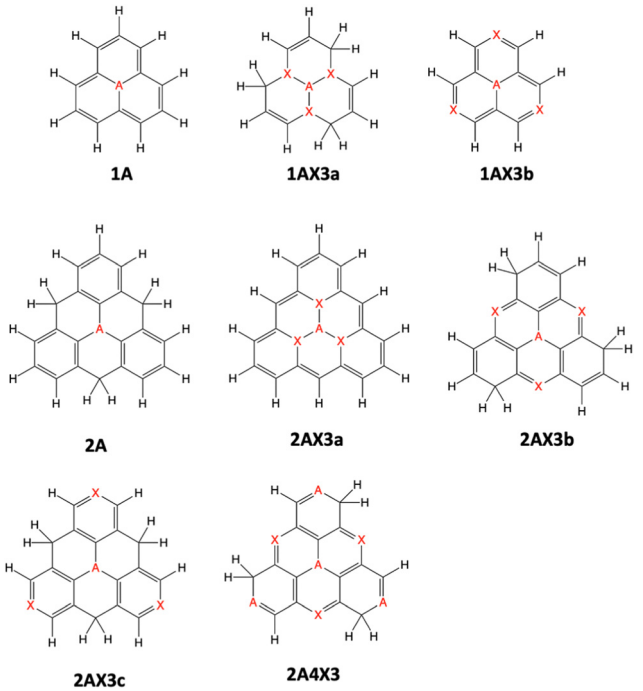

Fig. 1 Studied N and B doped phenalenes and triangulenes with (A,X) = (B,N) or (A,X) = (N,B).

2.3 Electronic structure calculations

Geometry optimization of the t16 studied molecules has been performed with the M06-2X exchange–correlation functional[38] and the 6-31G(d) basis set, as it has shown good performance in the study of planar conjugated compounds.[39–43] Transition energies to the low-lying excited singlet and triplet states have been computed at the time-dependent DFT (TDDFT) level with the Tamm–Dancoff approximation (TDA)[44] in combination with three exchange–correlation functionals: M06-2X,[38] B3LYP,[45–47] and CAM-B3LYP.[48] Excitation energies have been also computed at the spin–flip TDDFT (SF-TDDFT)[49] level (within the TDA) from the Kohn–Sham triplet state configuration with the PBE50 functional,[50] as previously recommended.[51] Several post Hartree–Fock (HF) approaches have been employed: configuration interaction singles with perturbative doubles (CIS(D))[52,53] with the resolution-of-the-identity (RI),[54] equation-of-motion coupled-cluster singles and doubles (EOM-CCSD),[55] and similarity transformed EOM domain-based local pair natural orbital CCSD (STEOM-DLPNO-CCSD).[56–58] Vertical excitation energies have been computed with the def2-TZVP basis set except for those at the SF-PBE50 level that were obtained with the 6-31G(d) basis set. SOCs have been computed at the STEOM-DLPNO-CCSD/def2-TZVP level within the mean-field approach for the two-electron part as implemented in ORCA.[59] Geometry optimizations, TDDFT and SF-TDDFT (TDA), CIS(D), and EOM-CCSD calculations have been done with the Q-Chem program.[60] STEOM-DLPNO-CCSD results were obtained with the use of the RI approach for Coulomb integrals (RI-J)[61] and the numerical chain-of-sphere integration for the HF exchange integrals (COSX)[62] with ORCA.

Along the manuscript, we consider three constant values for the triplet–triplet vibronic couplings in eqn (3): 1 meV (weak coupling), 10 meV (medium coupling), and 100 meV (strong coupling). The reorganization energy factor λ within the Marcus approximation (eqn (6)) has been fixed to 0.1 eV for all cases, as it is a common value in organic chromophores.[63,64] State populations of (nearly) degenerated triplets have been obtained according to the Boltzmann distribution at T = 298.15 K.

3 Results and discussion

3.1 Method assessment

The singlet–triplet energy difference is a key parameter determining the kinetics of rISC. Therefore, the computational design and characterization of molecules with efficient rISC requires the use of electronic structure methods able to accurately predict singlet and triplet excitation energies. Accordingly, we firstly evaluate the performance of DFT-based and post-HF wave function methods in the calculation of S_1 and T_1 energies of the doped phenalenes and triangulenes in Fig. 1.

Singlet–triplet energy gaps computed with different methods are shown in Fig. 2. Overall, the ΔE_{ST} values indicate small (or even negative) gaps for several doped compounds, particularly for structures: **1A**, **1AX3b**, **2AX3a**, **2AX3b**, **2NB3c** and **2A4X3**. On the other hand, the large energy differences (ΔE_{ST} > 0.5 eV) obtained for **1AX3a**, **2A** and **2BN3c** seem to prevent their rISC capabilities.

Although the general trend for ΔE_{ST} computed along the studied family of compounds is qualitatively the same for the different approaches, some values present large quantitative disagreements. TDDFT gaps computed with the hybrid GGA (B3LYP), LRC (CAM-B3LYP) and hybrid *meta*-GGA (M06-2X) functionals are rather close to STEOM-DLPNO-CCSD for large (and positive) ΔE_{ST} values, especially with CAM-B3LYP. On the other hand, none of the functionals is able to produce inverted gaps, and exhibit large discrepancies with respect to post-HF energies with $\Delta E_{ST} < 0$. Such behavior can be anticipated by the limitation of (linear response) TDDFT within the adiabatic approximation to account for the contribution of double excitations, which are known to stabilize the lowest excited singlet[65] and might be necessary in order to accurately provide relative energies between low-lying states,[66] as it has been recently reported for organic molecules with small or inverted singlet–triplet gaps.[19,67,68] To further corroborate the importance of double excitations in some of these molecules, in Table S4 (ESI†) we compare CIS *vs.* CIS(D) singlet and triplet energies for molecule **2B4N3** (large overestimation of singlet–triplet gap by TDDFT) and **1NB3a** (similar performance of TDDFT and post-HF).

In addition, we have also performed SF-TDDFT calculations. A priory, one advantage of employing the spin–flip excitation operator in TDDFT, as opposed to the standard linear-response approach, lies in its explicit incorporation of double excitations.[51] However, the high symmetry of the studied molecules (D_{3h} or C_{3h}, Table S1, ESI†) induces orbital

Open Access Article. Published on 25 März 2024. Downloaded on 06.02.26 16:58:20.
This article is licensed under a Creative Commons Attribution 3.0 Unported Licence.

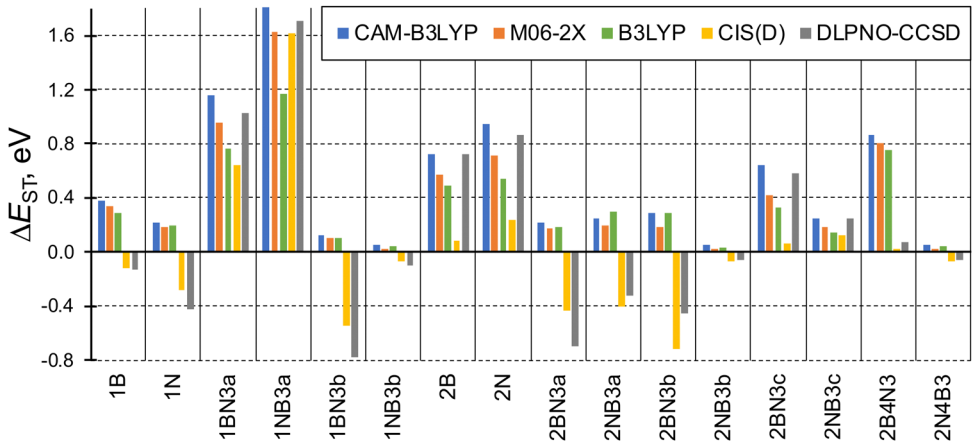

Fig. 2 Computed energy gaps between the lowest excited singlet and triplet states ($\Delta E_{ST} = E(S_1) - E(T_1)$, in eV) of the studied molecules. Note: DLPNO-CCSD refers to STEOM-DLPNO-CCSD.

degeneracies at the frontier between occupied and unoccupied levels. Consequently, in many cases, the lowest triplet state lacks a well-defined single configuration. This results in a rather pronounced singlet–triplet mixed character, *i.e.*, spin contamination, in both the reference triplet and the states computed using the SF-TDDFT approach. As a consequence, the results obtained with SF-TDDFT can be found in Table S2 (ESI†), but will not be further discussed here.

Amongst the different employed methods, only the two post-HF approaches are able to produce inverted singlet–triplet gaps ($\Delta E_{ST} < 0$), which we relate (again) to the larger impact of double excitations in S_1. On the other hand, CIS(D) energies in general follow the same trend as those obtained with STEOM-DLPNO-CCSD, although in some cases the differences are notably large, *e.g.*, in **2BN3c**.

These results make us to discard DFT-based methods (TDDFT and SF-TDDFT) for the study of rISC in B,N-doped triangulenes, as they seem to systematically overestimate ΔE_{ST} as compared to correlated wave function methods. Moreover, the variability between the post-HF methods motivates us to explore their accuracy in more detail. For that, we compare singlet and triplet excitation energies in compound **1B** at the CIS(D) and STEOM-DLPNO-CCSD levels with respect to highly accurate calculations, *i.e.*, EOM-CCSD and ADC(3) (Table 1).

The energy gap between the lowest singlet and triplet states in **1B** remains small across all post-HF approaches. EOM-CCSD predicts S_1 to be higher in energy than T_1, while the singlet–triplet gap is inverted in ADC(3). Notably, EOM-CCSD excels in calculating excitation energies for states predominantly governed by single electron excitations,[70] but its accuracy diminishes when double excitations are involved. Consequently, in cases like this, the inclusion of triple excitations, as in ADC(3), may yield a more balanced evaluation of ΔE_{ST}.

Interestingly, CIS(D) and STEOM-DLPNO-CCSD gaps are in very good agreement with ADC(3), with STEOM-DLPNO-CCSD displaying S_1 and T_1 energies closer to those from ADC(3). The accuracy in computing higher triplet states is also crucial for our study, as they can serve as mediators in the rISC process (eqn (3)). CIS(D) and STEOM-DLPNO-CCSD T_2 energies exhibit a 0.3 eV discrepancy compared to EOM-CCSD.

Based on the analysis of energies presented in Table 1, we conclude that STEOM-DLPNO-CCSD provides the most reliable excitation energies among the two considered post-HF methods with low computational demands. Furthermore, while CIS(D) incorporates effects of doubly excited configurations perturbatively, STEOM-DLPNO-CCSD explicitly accounts for (coupled-cluster) double excitations, all while maintaining an affordable computational expense. Consequently, we conduct our computational study of rISC in doped triangulenes using the STEOM-DLPNO-CCSD level of theory. For consistency, singlet–triplet SOCs have been computed at the same level.

Table 1 Post-HF excitation energies to the low-lying singlet and triplet states, and $\Delta E_{ST} = E(S_1) - E(T_1)$ in **1B** molecule. All values in eV

Method	ΔE_{ST}	$E(S_1)$	$E(T_1)$	$E(T_2)$
CIS(D)	−0.12	1.26	1.38	2.61
STEOM-DLPNO-CCSD	−0.13	0.80	0.93	2.02
EOM-CCSD	0.19	1.32	1.13	2.28
ADC(3)[a]	−0.10	0.55	0.65	—

[a] From ref. 69.

3.2 Direct *vs.* mediated rISC mechanisms

The conditions necessary for populating the excited singlet state *via* thermally activated rISC include a small singlet–triplet energy difference (ΔE_{ST}), typically on the order of k_BT, and a non-vanishing coupling between the initial and final states. Fig. 3a displays the computed ΔE_{ST} for the 16 doped phenalenes and triangulenes. Most of these molecules exhibit relatively modest gaps between the lowest excited singlet and triplet states, as calculated using the STEOM-DLPNO-CCSD method. While small and positive gaps can be overcome with thermal energy, rISC becomes energetically prohibitive in molecules with a large S_1/T_1 energy separation, such as **1BN3a** and **1NB3a**. Notably, several of them feature an inverted gap ($\Delta E_{ST} < 0$), which may serve as a driving force for rISC.

 This journal is © the Owner Societies 2024

Open Access Article. Published on 25 März 2024. Downloaded on 06.02.26 16:58:20.
This article is licensed under a Creative Commons Attribution 3.0 Unported Licence.

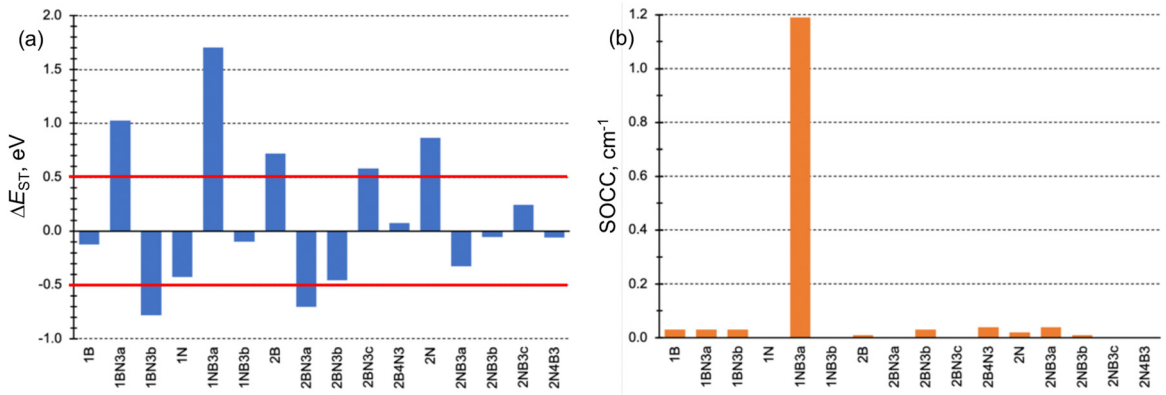

Fig. 3 (a) Excited singlet–triplet energy gaps (ΔE_{ST} in eV) and (b) SOC constants (SOCC in cm^{-1}) for the studied B and N doped phenalene and triangulene molecules.

However, excessively negative ΔE_{ST} values could impede fast rISC, as predicted by eqn (6).

The SOC constants (SOCCs) between S_1 and T_1 are generally quite small (SOCC $<$ 0.1 cm^{-1}) in almost all molecules (Fig. 3b). This observation aligns with expectations for organic π-conjugated molecules.[71] The exception to this behavior is **1NB3a** compound, which exhibits a considerably stronger coupling (SOCC $\approx$ 1.2 cm^{-1}) due to the different electronic character of S_1 (nπ*) and T_1 (ππ*) states, in agreement with the El-Sayed's rule.[72]

In the following, we investigate the rISC rates and analyze the main mechanisms in place. These include the direct population of S_1 *via* SOC (eqn (2)), as well as the mediation through auxiliary triplet states *via* the spin–vibronic mechanism (eqn (3)). We focus on molecules with not too large singlet–triplet gaps, $|\Delta E_{ST}| < 0.5$ eV (Fig. 4). Instead of explicitly computing triplet–triplet vibronic interactions ($\langle T_n|\hat{H}_{vib}|T_1\rangle$), we consider three distinct coupling regimes: weak (1 meV), medium (10 meV), and strong (100 meV). Changes in the strength of vibronic couplings may arise from various factors, including different chemical substitutions or varying environmental conditions, such as solvent polarity or molecular aggregation.

Representation of direct rISC rates (orange bars in Fig. 4) clearly highlights compounds with small ΔE_{ST} and nonzero S_1/T_1 SOCs. Notably, **1B**, **2NB3b**, **2B4N3**, and **2NB3a** exhibit the highest $k_{rISC}^{(d)}$ values. In contrast, molecules **1N**, **1NB3b**, and **2N4B3** possess vanishing SOC between S_1 and T_1 states, completely impeding the direct $T_1 \rightarrow S_1$ transition. Alternatively, rISC mediated by higher triplet states can be rather efficient.

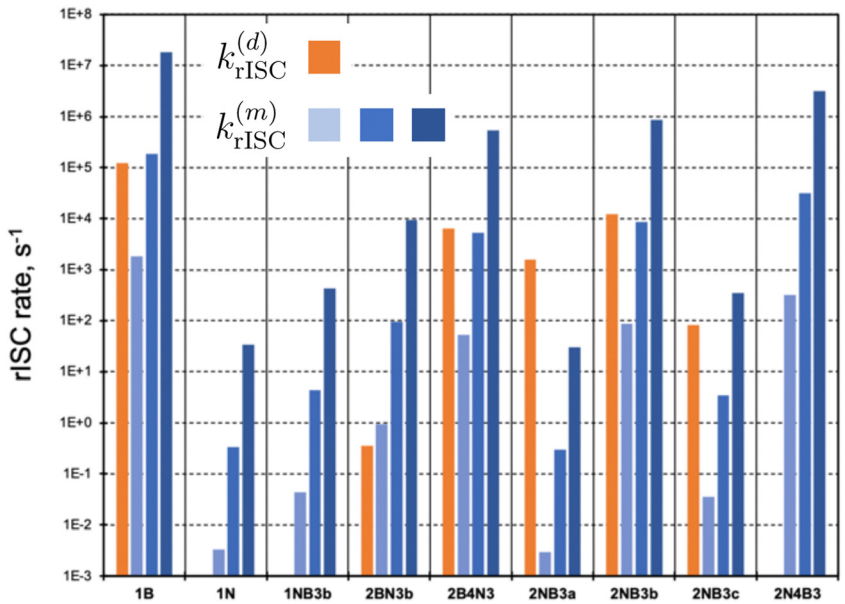

Fig. 4 Direct (*d*) and mediated (*m*) rate constants (in s^{-1}) for molecules with $|\Delta E_{ST}| < 0.5$ eV. $k_{rISC}^{(m)}$ has been computed for weak (1 meV, light blue), medium (10 meV, blue), and strong (100 meV, dark blue) vibronic couplings, respectively. Intermediate values to compute direct and mediated rates can be found in Table S5 (ESI†).

Open Access Article. Published on 25 Märerz 2024. Downloaded on 06.02.26 16:58:20.
This article is licensed under a Creative Commons Attribution 3.0 Unported Licence.

Specifically, in addition to those molecules with $\langle S_1|\hat{H}_{SOC}|T_1\rangle = 0$, the spin–vibronic mechanism dominates in **2BN3b**, even in the weak vibronic regime.

Remarkably, the excited triplet state predominantly contributing to $k_{rISC}^{(m)}$ is not necessarily T_2. In most cases, these correspond to T_4–T_6, as they exhibit rather strong SOC with S_1, while not being too high in energy. These findings underscore the importance of considering multiple triplets beyond T_1 to thoroughly evaluate the role of the spin–vibronic mechanism.

Interestingly, in many instances, the direct and spin–vibronic mechanisms may have similar magnitudes, contingent on the vibronic coupling strength. It is crucial to note that our approach does not account for quantum interference effects between both paths, which could result in a synergistic increase or decrease of rISC rates.

3.2.1 Singlet–triplet energy gap. The energy difference between excited singlet and triplet states characterized by the same (spatial) electronic transition is dictated (for the most part) by the exchange interaction between the hole and electron of the transition. If both excitations are dominated by a single orbital-to-orbital contribution, it corresponds to the exchange integral between these occupied and virtual orbitals.[65] The magnitude of the exchange integral is proportional to the orbital overlap, which can be used as a simple proxy to predict and rationalize ΔE_{ST}.

The impact of the orbital overlap is nicely illustrated by the comparison between the ΔE_{ST} values in **1BN3a** and **2N4B3** compounds. The lowest singlet and triplet excited states in **1BN3a** have a $\pi\pi^*$ character mainly corresponding to the excitation between doubly degenerated (e″) HOMO and LUMO+1 (Fig. 5). Both e″-orbital pairs are delocalized over the entire molecule with major participation of 2p orbitals from the same atomic centers, *i.e.*, non-disjoint orbitals, resulting in a rather large singlet–triplet gap (ΔE_{ST} = 1.02 eV, Fig. 3a). On the other hand, excitation to T_1 and S_1 in **2N4B3** arise from the electron promotion from the π-HOMO mostly localized on the C atoms bonded to the three B atoms, to the n-LUMO with major participation of the empty lone-pairs of the borons. Hence, the overlap in this case is much weaker, which explains the very small gap computed between T_1 and S_1 (ΔE_{ST} = −0.06 eV, Fig. 3a).

3.2.2 Singlet–triplet SOC. Besides a small ΔE_{ST}, rISC requires a sizeable SOC between the initial triplet and the final singlet states. For non-zero SOC, the product of the irreducible representations (irreps) of the spatial wave functions of the triplet and singlet, and the angular momentum (L_q, q = x,y,z) must contain the totally symmetric representation of the group.[73] This symmetry-based selection rule crystallizes to the El Sayed's rules[72] when applied to organic π-chromophores.

To exemplify the role of molecular symmetry in rISC, in the following, we analyze singlet–triplet computed SOCs in **1N** (D_{3h} structure) and **1B** (C_{3h} structure). The lowest singlet and triplet states in **1N** are obtained as the single electron promotion from one of the doubly degenerated HOMOs (e″) to the LUMO (a_2''), resulting in E' irrep for both states (Fig. 6). Since S_1 and T_1 belong to the same component of the twofold E' irrep, their product contain E' and A_1', but not A_2', while the componets of $\{L_q\}$ belong to the (E'', A_2') irreps. As a consequence, $\Gamma(S_1) \times \Gamma(L_q) \times \Gamma(T_1)$ does not contain the totally symmetric irrep (A_1'), resulting in zero T_1/S_1 SOC and forbidden rISC through the direct mechanism ($k_{rISC}^{(d)}$ = 0 in Fig. 4). On the other hand, the molecular symmetry in **1B** reduces to C_{3h} with the HOMO and LUMO exhibiting the same symmetry (a''). Therefore, S_1 and T_1 (both corresponding to the HOMO → LUMO excitation) belong to the A' irrep, with angular momentum components with (E'', A') symmetries, and $\Gamma(S_1) \times \Gamma(L_q) \times \Gamma(T_1) = (E'', A')$, allowing for non-zero SOC and efficient direct rISC.

As discussed in the previous section, the mediated (spin–vibronic) mechanism might be crucial in some of these doped triangulenes, in which the relevant spin–orbit interaction takes place between the lowest singlet and some higher triplet state (T_n). This is the situation in molecule **1N**, for which we have seen how the SOC between S_1 and T_1 is symmetry forbidden, while the S_1/T_6 coupling is quite strong (3.5 cm^{-1}). This behavior can be understood by the πn* nature of T_6 (Fig. 6), in accordance to El Sayed rule, opening the possibility for spin–vibronic rISC ($k_{rISC}^{(m)} > 0$ in Fig. 4).

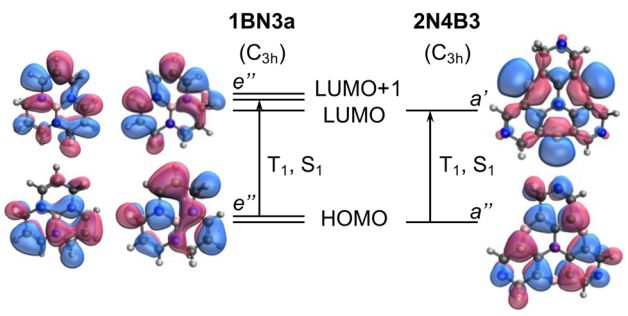

Fig. 5 Frontier molecular orbital diagram of molecules **1BN3a** (left) and **2N4B3** (right). Vertical arrows indicate orbital transition to T_1 and S_1 states.

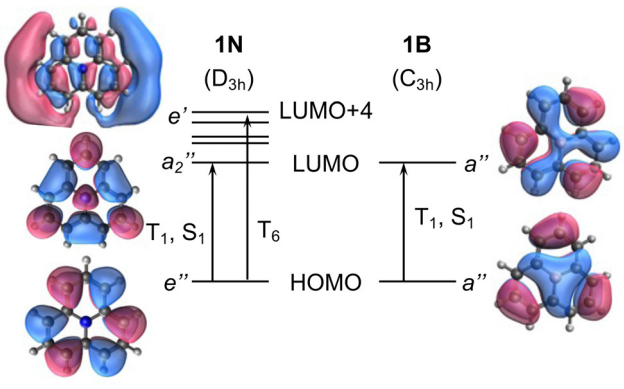

Fig. 6 Frontier molecular orbital diagram of molecules **1N** (left) and **1B** (right). Vertical arrows indicate orbital transition to low-lying excited states.

This journal is © the Owner Societies 2024

Open Access Article. Published on 25 März 2024. Downloaded on 06.02.26 16:58:20.
This article is licensed under a Creative Commons Attribution 3.0 Unported Licence.

3.3 Promising doped triangulenes

The results depicted in Fig. 3 and 4 provide valuable insights into the molecular structures with the most promising rISC capabilities.

Within a given molecular scaffold and doping pattern (Fig. 1), those structures with a greater number of B atoms than N dopants generally exhibit more efficient rISC. An exception to this trend is observed in the **2A4X3** structure, which deviates from the expected behavior among compounds with a relatively small singlet–triplet gap ($|\Delta E_{ST}| < 0.5$ eV). In this case, **2B4N3** and **2N4B3** present rates of similar magnitude.

The dependence of rISC efficiency on molecular size is strongly linked to the degree of π-conjugation within the molecule. Typically in these systems, larger conjugation tends to stabilize the S_1 state more than the T_1 state, resulting in a decrease of the ΔE_{ST} value and effecting the rISC capabilities. For example, **2AX3a** molecules exhibit smaller energy gaps compared to their **1AX3a** counterparts. Consequently, while **1NB3a** exhibits a prohibitively large ΔE_{ST}, **2NB3a** is predicted to have efficient rISC. Conversely, the increase in molecular size from **1A** to **2A** results in a loss of effective conjugation, leading to overly large energy gaps in the latter compounds (**2B** and **2N**). The substitution of the phenalene scaffold with triangulene between **1AX3b** and **2AX3b** structures implies a moderate increase in conjugation, causing not very large changes in ΔE_{ST}, yet having a significant impact on their rISC efficiencies, as observed between **1NB3b** and **2NB3b**.

The distribution of dopant atoms in the molecule also significantly influences the photophysical properties, as evidenced in the **2AX3a**, **2AX3b**, and **2AX3c** series of compounds. Specifically, larger separations between dopant atoms A and X (N and B or B and N) result in larger singlet–triplet gaps, making the **2AX3b** structure optimal for efficient rISC. This behavior can be rationalized in terms of molecular conjugation, which decreases as **2AX3a** > **2AX3b** > **2AX3c**.

While it is not entirely clear to establish a direct correlation between ΔE_{ST} or rISC rate and the amount of doping, overall, a larger number of dopants appears to be beneficial in promoting rISC, as exemplified in the **2A**, **2AX3b**, and **2A4X3** series of compounds.

4 Conclusions

In summary, our study of 16 nitrogen and/or boron-doped triangulene nanographene molecules has provided crucial insights into the appropriateness of electronic structure methods for unraveling the intricacies of rISC mechanisms and assessing their efficiencies.

Comparison between singlet and triplet energies of the studied systems advises the use of post-HF methods accounting for double excitations. These contributions have a larger impact on the excited singlet energy, reducing the singlet–triplet gap, which for some molecules appears to be inverted ($\Delta E_{ST} < 0$). Comparison with reference calculations including triplet excitations, that is at the ADC(3) level, makes us to conclude that STEOM-DLPNO-CCSD with the def2-TZVP basis set is a suitable method for the present study. Moreover, we believe that this approach should be rather accurate for the study of MR-TADF organic molecules in general. On the other hand, TDDFT calculations with different families of exchange–correlation functionals produce systematically larger and always positive ΔE_{ST} values. Although SF-TDDFT explicitly contains double excitations, it cannot be used to describe the doped phenalenes and triangulenes studied here due to the large spin-mixed character of the computed states, which we attribute to the high symmetry (D_{3h} or C_{3h}) of the compounds. Hence, despite the advantageous computational cost of DFT-based methods, we cannot consider them as appropriate for the accurate calculation of singlet–triplet energies.

Symmetry selection rules in many cases hinders SOC from T_1 to S_1, inactivating direct rISC. Contrarily, the spin–vibronic (mediated) mechanism, computed as a second order perturbation term, is extremely relevant for the population of the triplet manifold in all doped nanographenes with small to moderate singlet–triplet gaps. Notably, in many molecules, the triplet state mediator is not the energetically closest one to T_1 (or S_1), which imposes the need to take into account several highly excited triplets, *i.e.*, beyond T_2, in computational studies.

While a clear correlation between ΔE_{ST} or rISC rate and doping amount is not established, a larger number of dopants generally promotes efficient rISC. Our calculations also indicate that triangulenes with more B atoms than N atoms generally exhibit more efficient rISC, with dopant atom distribution also impacting the performance. Moreover, the degree of π-conjugation is a very important factor for rISC, as it tunes the singlet–triplet energy gap, with larger conjugation stabilizing S_1 over T_1.

In summary, our comprehensive analysis sheds light on the factors influencing rISC in doped triangulene molecules, providing valuable guidance for the design of efficient MR-TADF compounds.

Data availability

The data that supports the findings of this study are available within the article and its ESI.†

Conflicts of interest

The authors declare that they have no conflict of interest.

Acknowledgements

The authors thank Gaetano Ricci for very insightful and helpful discussions. The authors acknowledge the Spanish Government MICINN (projects PID2022-136231NB-I00 and RED2022-134939-T) and the Eusko Jaurlaritza (Basque Government, project IT1584-22). D. C. is thankful for financial support from IKERBASQUE (Basque Foundation for Science). The authors are thankful for the technical and human support provided by the Donostia International Physics Center (DIPC) Computer Center.

Open Access Article. Published on 25 Mäerz 2024. Downloaded on 06.02.26 16:58:20.
This article is licensed under a Creative Commons Attribution 3.0 Unported Licence.

References

1 A. Bernanose, M. Comte and P. Vouaux, Sur un nouveau mode d'émission lumineuse chez certains composés organiques, *J. Chim. Phys.*, 1953, **50**, 64–68.
2 C. W. Tang and S. A. VanSlyke, Organic electroluminescent diodes, *Appl. Phys. Lett.*, 1987, **51**, 913–915.
3 H.-W. Chen, J.-H. Lee, B.-Y. Lin, S. Chen and S.-T. Wu, Liquid crystal display and organic light-emitting diode display: present status and future perspectives, *Light Sci. Appl.*, 2018, **7**, 17168.
4 M. A. Baldo, D. F. O'Brien, Y. You, A. Shoustikov, S. Sibley, M. E. Thompson and S. R. Forrest, Highly efficient phosphorescent emission from organic electroluminescent devices, *Nature*, 1998, **395**, 151–154.
5 M. Baldo, S. Lamansky, P. Burrows, M. Thompson and S. Forrest, Very high-efficiency green organic light-emitting devices based on electrophosphorescence, *Appl. Phys. Lett.*, 1999, **75**, 4–6.
6 M. Thompson; P. Djurovich; S. Barlow and S. Marder, *Organometallic Complexes for optoelectronic applications*, 2007.
7 R. Kepler, J. Caris, P. Avakian and E. Abramson, Triplet excitons and delayed fluorescence in anthracene crystals, *Phys. Rev. Lett.*, 1963, **10**, 400.
8 B. Valeur and M. N. Berberan-Santos, *Molecular fluorescence: principles and applications*, John Wiley & Sons, 2012.
9 T. Nakagawa, S.-Y. Ku, K.-T. Wong and C. Adachi, Electroluminescence based on thermally activated delayed fluorescence generated by a spirobifluorene donor–acceptor structure, *Chem. Commun.*, 2012, **48**, 9580–9582.
10 D. S. M. Ravinson and M. E. Thompson, Thermally assisted delayed fluorescence (TADF): Fluorescence delayed is fluorescence denied, *Mater. Horiz.*, 2020, **7**, 1210–1217.
11 Z. Yang, Z. Mao, Z. Xie, Y. Zhang, S. Liu, J. Zhao, J. Xu, Z. Chi and M. P. Aldred, Recent advances in organic thermally activated delayed fluorescence materials, *Chem. Soc. Rev.*, 2017, **46**, 915–1016.
12 H. Uoyama, K. Goushi, K. Shizu, H. Nomura and C. Adachi, Highly efficient organic light-emitting diodes from delayed fluorescence, *Nature*, 2012, **492**, 234–238.
13 Y. Tao, K. Yuan, T. Chen, P. Xu, H. Li, R. Chen, C. Zheng, L. Zhang and W. Huang, Thermally activated delayed fluorescence materials towards the breakthrough of organoelectronics, *Adv. Mater.*, 2014, **26**, 7931–7958.
14 M. K. Etherington, J. Gibson, H. F. Higginbotham, T. J. Penfold and A. P. Monkman, Revealing the spin–vibronic coupling mechanism of thermally activated delayed fluorescence, *Nat. Commun.*, 2016, **7**, 1–7.
15 Y. Olivier, B. Yurash, L. Muccioli, G. D'Avino, O. Mikhnenko, J.-C. Sancho-Garcia, C. Adachi, T.-Q. Nguyen and D. Beljonne, Nature of the singlet and triplet excitations mediating thermally activated delayed fluorescence, *Phys. Rev. Mater.*, 2017, **1**, 075602.
16 J. Gibson, A. P. Monkman and T. J. Penfold, The importance of vibronic coupling for efficient reverse intersystem crossing in thermally activated delayed fluorescence molecules, *ChemPhysChem*, 2016, **17**, 2956–2961.
17 T. Hatakeyama, K. Shiren, K. Nakajima, S. Nomura, S. Nakatsuka, K. Kinoshita, J. Ni, Y. Ono and T. Ikuta, Ultrapure blue thermally activated delayed fluorescence molecules: efficient HOMO–LUMO separation by the multiple resonance effect, *Adv. Mater.*, 2016, **28**, 2777–2781.
18 A. Pershin, D. Hall, V. Lemaur, J.-C. Sancho-Garcia, L. Muccioli, E. Zysman-Colman, D. Beljonne and Y. Olivier, Highly emissive excitons with reduced exchange energy in thermally activated delayed fluorescent molecules, *Nat. Commun.*, 2019, **10**, 1–5.
19 N. Aizawa, Y.-J. Pu, Y. Harabuchi, A. Nihonyanagi, R. Ibuka, H. Inuzuka, B. Dhara, Y. Koyama, K.-I. Nakayama and S. Maeda, *et al.*, Delayed fluorescence from inverted singlet and triplet excited states, *Nature*, 2022, **609**, 502–506.
20 A. L. Sobolewski and W. Domcke, Are heptazine-based organic light-emitting diode chromophores thermally activated delayed fluorescence or inverted singlet–triplet systems?, *J. Phys. Chem. Lett.*, 2021, **12**, 6852–6860.
21 X. Lv, J. Miao, M. Liu, Q. Peng, C. Zhong, Y. Hu, X. Cao, H. Wu, Y. Yang and C. Zhou, *et al.*, Extending the p-Skeleton of Multi-Resonance TADF Materials towards High-Efficiency Narrowband Deep-Blue Emission, *Angew. Chem., Int. Ed.*, 2022, **134**, e202201588.
22 P. Jiang, J. Miao, X. Cao, H. Xia, K. Pan, T. Hua, X. Lv, Z. Huang, Y. Zou and C. Yang, Quenching-resistant multi-resonance TADF emitter realizes 40% external quantum efficiency in narrowband electroluminescence at high doping level, *Adv. Mater.*, 2022, **34**, 2106954.
23 S. Kohata, H. Nakanotani, Y. Chitose, T. Yasuda, Y. Tsuchiya and C. Adachi, Anti-Stokes Luminescence in Multi-Resonance-Type Thermally-Activated Delayed Fluorescence Molecules, *Angew. Chem., Int. Ed.*, 2023, **62**, e202312326.
24 A. Carreras and D. Casanova, Theory of Exciton Dynamics in Thermally Activated Delayed Fluorescence, *ChemPhotoChem*, 2022, **6**, e202200066.
25 T. Ogiwara, Y. Wakikawa and T. Ikoma, Mechanism of intersystem crossing of thermally activated delayed fluorescence molecules, *J. Phys. Chem. A*, 2015, **119**, 3415–3418.
26 Y. Zhao, Y. Wu, W. Chen, R. Zhang, G. Hong, J. Tian, H. Wang, D. Zheng, C. Wu and X. Jiang, *et al.*, The Second Excited Triplet-State Facilitates TADF and Triplet–Triplet Annihilation Photon Upconversion via a Thermally Activated Reverse Internal Conversion, *Adv. Opt. Mater.*, 2022, **10**, 2102275.
27 P. L. Santos, J. S. Ward, P. Data, A. S. Batsanov, M. R. Bryce, F. B. Dias and A. P. Monkman, Engineering the singlet–triplet energy splitting in a TADF molecule, *J. Mater. Chem. C*, 2016, **4**, 3815–3824.
28 T. Förster, Excitation transfer and internal conversion, *Chem. Phys. Lett.*, 1971, **12**, 422–424.
29 Z. Wang, C. Wu and W. Liu, NAC-TDDFT: Time-Dependent Density Functional Theory for Nonadiabatic Couplings, *Acc. Chem. Res.*, 2021, **54**, 3288–3297.

 This journal is © the Owner Societies 2024

Open Access Article. Published on 25 Märerz 2024. Downloaded on 06.02.26 16:58:20.
This article is licensed under a Creative Commons Attribution 3.0 Unported Licence.

30 E. G. Hohenstein, Analytic formulation of derivative coupling vectors for complete active space configuration interaction wavefunctions with floating occupation molecular orbitals, *J. Chem. Phys.*, 2016, **145**, 174110.
31 H. Lischka, M. Dallos, P. G. Szalay, D. R. Yarkony and R. Shepard, Analytic evaluation of nonadiabatic coupling terms at the MR-CI level. I. Formalism, *J. Chem. Phys.*, 2004, **120**, 7322–7329.
32 I. Lengsfield, H. Byron, P. Saxe and D. R. Yarkony, On the evaluation of nonadiabatic coupling matrix elements using SA-MCSCF/CI wave functions and analytic gradient methods. I, *J. Chem. Phys.*, 1984, **81**, 4549–4553.
33 P. Saxe, B. H. Lengsfield and D. R. Yarkony, On the evaluation of non-adiabatic coupling matrix elements for large scale CI wavefunctions, *Chem. Phys. Lett.*, 1985, **113**, 159–164.
34 S. Faraji, S. Matsika and A. I. Krylov, Calculations of non-adiabatic couplings within equation-of-motion coupled-cluster framework: Theory, implementation, and validation against multi-reference methods, *J. Chem. Phys.*, 2018, **148**, 044103.
35 X. Zhang and J. M. Herbert, Analytic derivative couplings for spin-flip configuration interaction singles and spin-flip time-dependent density functional theory, *J. Chem. Phys.*, 2014, **141**, 064104.
36 Q. Peng, Y. Niu, Q. Shi, X. Gao and Z. Shuai, Correlation Function Formalism for Triplet Excited State Decay: Combined Spin–Orbit and Nonadiabatic Couplings, *J. Chem. Theory Comput.*, 2013, **9**, 1132–1143.
37 R. A. Marcus, Electron transfer reactions in chemistry. Theory and experiment, *Rev. Mod. Phys.*, 1993, **65**, 599.
38 Y. Zhao and D. G. Truhlar, The M06 suite of density functionals for main group thermochemistry, thermochemical kinetics, noncovalent interactions, excited states, and transition elements: two new functionals and systematic testing of four M06-class functionals and 12 other functionals, *Theor. Chem. Acc.*, 2008, **120**, 215–241.
39 D. Josa, J. Rodríguez-Otero, E. M. Cabaleiro-Lago and M. Rellán-Piñeiro, Analysis of the performance of DFT-D, M05-2X and M06-2X functionals for studying p···p interactions, *Chem. Phys. Lett.*, 2013, **557**, 170–175.
40 A. Pérez-Guardiola, M. E. Sandoval-Salinas, D. Casanova, E. San-Fabián, A. J. Pérez-Jiménez and J. C. Sancho-García, The role of topology in organic molecules: origin and comparison of the radical character in linear and cyclic oligoacenes and related oligomers, *Phys. Chem. Chem. Phys.*, 2018, **20**, 7112–7124.
41 T. Wang, A. Berdonces-Layunta, N. Friedrich, M. Vilas-Varela, J. P. Calupitan, J. I. Pascual, D. Peña, D. Casanova, M. Corso and D. G. de Oteyza, Aza-Triangulene: On-Surface Synthesis and Electronic and Magnetic Properties, *J. Am. Chem. Soc.*, 2022, **144**, 4522–4529.
42 M. Vilas-Varela, *et al.*, On-Surface Synthesis and Characterization of a High-Spin Aza-[5]-Triangulene, *Angew. Chem., Int. Ed.*, 2023, **62**, e202307884.
43 T. Wang, P. Angulo-Portugal, A. Berdonces-Layunta, A. Jancarik, A. Gourdon, J. Holec, M. Kumar, D. Soler, P. Jelinek, D. Casanova, M. Corso, D. G. de Oteyza and J. P. Calupitan, Tuning the Diradical Character of Pentacene Derivatives *via* Non-Benzenoid Coupling Motifs, *J. Am. Chem. Soc.*, 2023, **145**, 10333–10341.
44 S. Hirata and M. Head-Gordon, Time-dependent density functional theory within the Tamm–Dancoff approximation, *Chem. Phys. Lett.*, 1999, **314**, 291–299.
45 K. Kim and K. Jordan, Comparison of density functional and MP2 calculations on the water monomer and dimer, *J. Phys. Chem.*, 1994, **98**, 10089–10094.
46 P. J. Stephens, F. J. Devlin, C. F. Chabalowski and M. J. Frisch, *Ab initio* calculation of vibrational absorption and circular dichroism spectra using density functional force fields, *J. Phys. Chem.*, 1994, **98**, 11623–11627.
47 C. J. Cramer, *Computational Chemistry, Theories and Models*, 2004.
48 T. Yanai, D. P. Tew and N. C. Handy, A new hybrid exchange–correlation functional using the Coulomb-attenuating method (CAM-B3LYP), *Chem. Phys. Lett.*, 2004, **393**, 51–57.
49 Y. Shao, M. Head-Gordon and A. I. Krylov, The spin–flip approach within timedependent density functional theory: Theory and applications to diradicals, *J. Chem. Phys.*, 2003, **118**, 4807–4818.
50 Y. A. Bernard, Y. Shao and A. I. Krylov, General formulation of spin-flip time-dependent density functional theory using non-collinear kernels: Theory, implementation, and benchmarks, *J. Chem. Phys.*, 2012, **136**, 204103.
51 D. Casanova and A. I. Krylov, Spin-flip methods in quantum chemistry, *Phys. Chem. Chem. Phys.*, 2020, **22**, 4326–4342.
52 M. Head-Gordon, D. Maurice and M. Oumi, A perturbative correction to restricted open shell configuration interaction with single substitutions for excited states of radicals, *Chem. Phys. Lett.*, 1995, **246**, 114–121.
53 M. Head-Gordon, R. J. Rico, M. Oumi and T. J. Lee, A doubles correction to electronic excited states from configuration interaction in the space of single substitutions, *Chem. Phys. Lett.*, 1994, **219**, 21–29.
54 Y. M. Rhee and M. Head-Gordon, Scaled second-order perturbation corrections to configuration interaction singles: Efficient and reliable excitation energy methods, *J. Phys. Chem. A*, 2007, **111**, 5314–5326.
55 A. I. Krylov, Size-consistent wave functions for bond-breaking: The equation-ofmotion spin-flip model, *Chem. Phys. Lett.*, 2001, **338**, 375–384.
56 M. Nooijen and R. J. Bartlett, A new method for excited states: Similarity transformed equation-of-motion coupled-cluster theory, *J. Chem. Phys.*, 1997, **106**, 6441–6448.
57 C. Riplinger and F. Neese, An efficient and near linear scaling pair natural orbital based local coupled cluster method, *J. Chem. Phys.*, 2013, **138**, 034106.
58 R. Izsák, A local similarity transformed equation of motion approach for calculating excited states, *Int. J. Quantum Chem.*, 2021, **121**, e26327.
59 F. Neese, The ORCA program system, *Wiley Interdiscip. Rev.: Comput. Mol. Sci.*, 2012, **2**, 73–78.

Open Access Article. Published on 25 Mäerz 2024. Downloaded on 06.02.26 16:58:20.
This article is licensed under a Creative Commons Attribution 3.0 Unported Licence.

60 E. Epifanovsky, *et al.*, Software for the frontiers of quantum chemistry: An overview of developments in the Q-Chem 5 package, *J. Chem. Phys.*, 2021, **155**, 084801.
61 F. Neese, An improvement of the resolution of the identity approximation for the formation of the Coulomb matrix, *J. Comput. Chem.*, 2003, **24**, 1740–1747.
62 F. Neese, F. Wennmohs, A. Hansen and U. Becker, Efficient, approximate and parallel Hartree–Fock and hybrid DFT calculations. A 'chain-of-spheres' algorithm for the Hartree–Fock exchange, *Chem. Phys.*, 2009, **356**, 98–109.
63 X. Amashukeli, J. R. Winkler, H. B. Gray, N. E. Gruhn and D. L. Lichtenberger, Electron-transfer reorganization energies of isolated organic molecules, *J. Phys. Chem. A*, 2002, **106**, 7593–7598.
64 K. Chen, C. Kunkel, K. Reuter and J. T. Margraf, Reorganization energies of flexible organic molecules as a challenging target for machine learning enhanced virtual screening, *Digital Discovery*, 2022, **1**, 147–157.
65 M. E. Sandoval-Salinas, G. Ricci, A. Pérez-Jiménez, D. Casanova, Y. Olivier and J.-C. Sancho-Garcia, Correlation *vs.* exchange competition drives the singlet–triplet excited-state inversion in non-alternant hydrocarbons, *Phys. Chem. Chem. Phys.*, 2023, **25**, 26417–26428.
66 P.-F. Loos, A. Scemama and D. Jacquemin, The quest for highly accurate excitation energies: A computational perspective, *J. Phys. Chem. Lett.*, 2020, **11**, 2374–2383.
67 R. Pollice, P. Friederich, C. Lavigne, G. dos Passos Gomes and A. Aspuru-Guzik, Organic molecules with inverted gaps between first excited singlet and triplet states and appreciable fluorescence rates, *Matter*, 2021, **4**, 1654–1682.
68 P. de Silva, Inverted singlet–triplet gaps and their relevance to thermally activated delayed fluorescence, *J. Phys. Chem. Lett.*, 2019, **10**, 5674–5679.
69 A. Dreuw and M. Hoffmann, The inverted singlet–triplet gap: a vanishing myth?, *Front. Chem.*, 2023, **11**, 1239604.
70 A. I. Krylov, Equation-of-Motion Coupled-Cluster Methods for Open-Shell and Electronically Excited Species: The Hitchhiker's Guide to Fock Space, *Annu. Rev. Phys. Chem.*, 2008, **59**, 433–462.
71 C. M. Marian, Understanding and Controlling Intersystem Crossing in Molecules, *Annu. Rev. Phys. Chem.*, 2021, **72**, 617–640.
72 M. A. El-Sayed, Spin—Orbit Coupling and the Radiationless Processes in Nitrogen Heterocyclics, *J. Chem. Phys.*, 1963, **38**, 2834–2838.
73 D. G. Fedorov and M. S. Gordon, *Low-Lying Potential Energy Surfaces*, 2002, ch. 13, pp. 276–297.

 This journal is © the Owner Societies 2024